Spectroscopy and dynamics of jet-cooled hydrazines and ammonia. I. Single-photon absorption and ionization spectra

Jack A. Syage,[a] Ronald B. Cohen, and Jhobe Steadman[b]
The Aerospace Corporation, P. O. Box 92957/M5-754, Los Angeles, California 90009

(Received 11 May 1992; accepted 20 July 1992)

Electronic-state properties of hydrazine (N_2H_4), monomethyl hydrazine (MMH), unsymmetrical dimethyl hydrazine (UDMH), and ammonia were investigated by single-photon vacuum ultraviolet (vuv) absorption and photoionization spectroscopy in a molecular-beam apparatus. The photoionization spectrum of NH_3 shows a sharp threshold at a value of 10.16 eV in excellent agreement with previous measurements. The ionization thresholds of the hydrazines are very broad reflecting the large (nearly 2 eV) structural relaxation energy for conversion from a C_2 pyramidal *gauche* neutral geometry to a D_{2h} planar ion geometry. The measured threshold photoionization potentials are 8.32 eV (N_2H_4), 8.05 eV (MMH), and 7.87 eV (UDMH). The vuv absorption spectra of the hydrazines are also broad, which is to be contrasted with the well-resolved spectrum of NH_3. The band shapes can be attributed to planarization of the Rydberg excited states in analogy to the ion structure. A molecular-orbital model is developed to provide understanding of the excited states in terms of their symmetries, energy ordering, and selection rules, as a function of geometry.

I. INTRODUCTION

Hydrazines are a very important class of energetic molecules. They are storable liquids, which make them attractive as fuels for thrusters used in long-term satellite and space activities. At present, the spectroscopy and chemical dynamics of the hydrazines are poorly understood.[1–6] Virtually no electronic-state information is available, nor is there much understanding of photodissociation properties. This information is vital to understanding the dynamics of thrusters (kinetic-energy releases, fragment internal excitation) as well as spectral emissions from rocket plumes. These processes involve complex kinetics[7–10] which cannot be adequately studied without a basic understanding of the spectroscopy of the molecules involved. We are engaged in a program to increase the base of information for these molecules with the ultimate goal of understanding state-to-state energy disposal by thermal, photochemical, and bimolecular reactive decomposition.

In this paper we make use of a vacuum ultraviolet (vuv) supersonic-jet spectrometer configured for recording direct absorption spectra and photoionization efficiency spectra of cold molecules to a short-wavelength limit of about 120 nm (10.4 eV).[11] Measurements are reported for the series of molecules NH_3, H_2NNH_2 [hydrazine], $H_2NNH(CH_3)$ [monomethyl-hydrazine, MMH], and $H_2NN(CH_3)_2$ [unsymmetrical dimethylhydrazine, UDMH]. In the following paper, we report electron-impact dissociative-ionization cross sections and discuss dissociation mechanisms resulting from core–electron excitation.[12]

Electronic-state spectra of hydrazines are almost nonexistent. Schürgers and Welge[13] and Biehl and Stuhl[14] reported ambient absorption spectra of N_2H_4 to 120 nm showing a few broad and weakly defined bands. The spectra reported here show these same bands and reveal other weaker and/or overlapping absorptions. Vacuum ultraviolet absorption spectra of MMH and UDMH have not previously been reported. The spectra of the hydrazines as a group show a pattern of band shifts and intensities that assist greatly in assigning the transitions. Several *ab initio* calculations[15–20] have been reported for the ground state of N_2H_4 confirming experimental evidence[21–23] that the geometry is of C_2 symmetry with pyramidal nitrogen bonds and a N–N dihedral angle of about 95° (*gauche*) with respect to the nonbonding orbitals. Information on the unoccupied higher energy orbitals of N_2H_4 is scant.[24,25] Staemmler calculated the interaction of two nitrogen 3*s* orbitals in N_2H_4 and determined transition energies and oscillator strengths for 2*p* excitation.[24] However, the calculation was limited to C_2 geometry and no other excited states were considered. Based on the evidence for a planar (D_{2h}) $N_2H_4^+$ ion,[26–33] one might also expect a planar geometry for the Rydberg-type states of N_2H_4.

Geometry plays a major role in understanding hydrazine spectroscopy and dynamics. The stable C_2 *gauche* geometry of the neutral ground state is destabilized by ionization relative to the planar geometry. Single-photon ionization measurements of the jet-cooled hydrazines are reported here and are consistent with a difference in the vertical and adiabatic ionization potentials of about 2 eV. This difference, sometimes referred to as the structural relaxation energy ΔH_r, is unusually large. For example, this value is 0.70 eV for NH_3 ionization (or Rydberg excitation) involving the rather large change from pyramidal to planar geometry. The spectra reported here for the hydrazines also show that large geometry changes occur for electronic excitation below the ionization potential.

As part of our effort to assign the excited electronic-

[a]Author to whom correspondence should be sent.
[b]National Research Council postdoctoral associate. Current address is GeoCenters Inc., Gun Powder Branch, P.O. Box 68, Aberdeen Proving Grounds, Maryland 21010.

 0021-9606/92/216072-13$006.00

state bands, we present a simple model and then a more rigorous model to explain the large geometry changes that occur by excitation of an electron from a nonbonding orbital. A molecular-orbital correlation diagram is developed that identifies the major excited electronic states, estimates the relative energies for C_2 *gauche* vs D_{2h} planar geometries, and determines the optical selection rules for the mixed $C_2 \rightarrow D_{2h}$ transitions. Knowledge of electronic-state properties and potential energy surfaces is necessary to properly interpret reaction dynamics. The direction of this research is to understand bimolecular reactivity of hydrazines with electrons and atomic and molecular radicals. The first phase of work toward this goal is presented in the following paper (Paper II) where absolute dissociative-ionization cross sections, fragment appearance potentials, and fragment kinetic-energy distributions are presented for electron excitation of NH_3, N_2H_4, and MMH. The molecular-orbital picture developed here for hydrazine is used in Paper II to explain fragment thresholds, branching ratios, and reaction mechanisms in terms of excited-state energies and bonding-orbital excitations.

II. EXPERIMENT

A supersonic-jet absorption spectrometer was used to record electronic-state spectra and single-photon ionization efficiency curves. A schematic of the apparatus is given in Fig. 1. An earlier version of the apparatus for recording absorption spectra has been described before.[11] Significant improvements have been during the course of this work.

Vacuum chamber. The gas source is a solenoid-actuated pulsed valve that is aimed directly into a 1500 ℓ/s turbomolecular pump backed by a 16 ℓ/s direct-drive pump. An assembly containing two flat mirrors is mounted on the pulsed valve to achieve three passes of the light beam through the jet. The mirror substrates are coated with Al and a MgF_2 overcoat for optimum vuv reflectivity. Because a cw light source is used, it is advantageous to operate at high duty cycle within the constraints of the pumping system. We usually operate the pulsed valve at 50 Hz with a pulse width of 0.6–0.8 ms. The solenoid coil is water cooled. The use of a 500 μm aperture and 5–25 psi backing pressures of He or Ar generates a gas throughput in the range of 0.1–0.5 Torr ℓ/s. Typical ambient pressures in this work were 2×10^{-4} Torr for absorption measurements and 1×10^{-5} Torr (10 Hz) for ionization measurements.

Light source. A 30 W deuterium arc-discharge lamp with MgF_2 windows (Hamamatsu L879) is used as a broadband uv/vuv light source and is dispersed in a vacuum monochromator. The lamp exit window has a sufficiently long cylindrical region to allow a vacuum coupling to the monochromator in an arrangement much like a Cajon Ultra-Torr fitting. The measured spectral output in our apparatus is given in Fig. 2(a). A 0.2 m Seka-Namioka-type monochromator (40 Å/mm dispersion with a 1200 lines/mm grating) was originally used for these experiments, but was replaced by a 0.5 m Czerny–Turner-type monochromator (16 and 5 Å/mm dispersion, respectively,

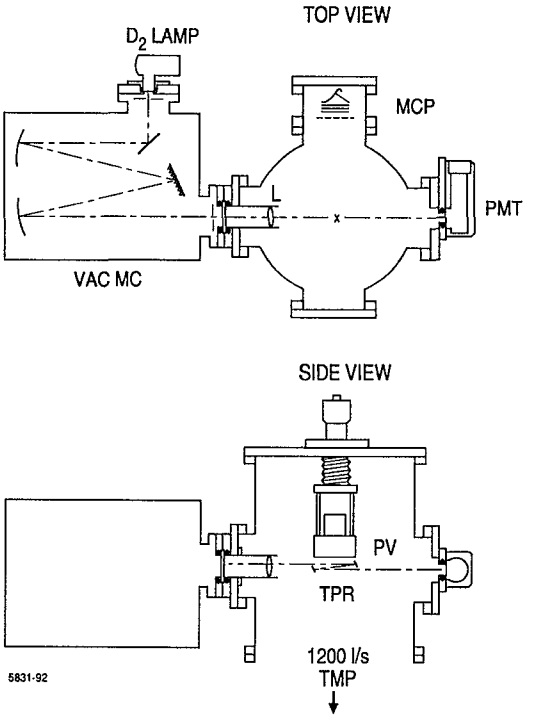

FIG. 1. Diagram of the supersonic-jet vuv absorption spectrometer. The × marks the crossing of the molecular jet and the light beam. The pulsed valve (PV) is at the top of the chamber and the gas output is directed into the turbomolecular pump (TMP). The photomultiplier tube (PMT) assembly translates down (side view) to accomodate the displacement of the light beam by the triple-pass reflector (TPR). The vacuum monochromator (VAC MC) is evacuated with a sorption pump. Other symbols are L—MgF_2 lens; MCP—microchannel plate detector. Drawing is not to scale.

with a 1200 or 3600 lines/mm grating) during the course of this work. Our apparatus can achieve 1–2 cm^{-1} resolution at 200 nm excitation with a 10 μ slit width, although we opted for better sensitivity and less resolution for this work. The monochromator is evacuated with a liquid-nitrogen-cooled sorption pump. A spherical lens is used to focus the slit-shaped output light to a rectangular dimension of about 4×2 mm with the long dimension parallel to the monochromator slit and the jet centerline. The light intensity is measured by photon counting using one of two methods. A MgF_2 exit window was coated with the scintillator sodium salicylate, which allows detection of light continuously from the visible to the vuv. We now employ a solar-blind photomultiplier tube (Hamamatsu R1220P) without scintillator, which significantly increases sensitivity, but limits detection to wavelengths less than 280 nm. The side-on photomultiplier tube has a MgF_2 window that is vacuum sealed to the chamber using a specially adapted mounting plate (Fig. 1).

Counting statistics. Absorption is detected by measuring the difference in light intensity for two gated time intervals, one which overlaps with the gas pulse (I) and the other which is delayed by about 4 ms (I_0). The gate widths are typically 1 ms and the pulse-pair resolution for photon counting is $\tau_{res}=10$ ns. A high count rate improves sensitivity, but can lead to counting error due to double strikes.

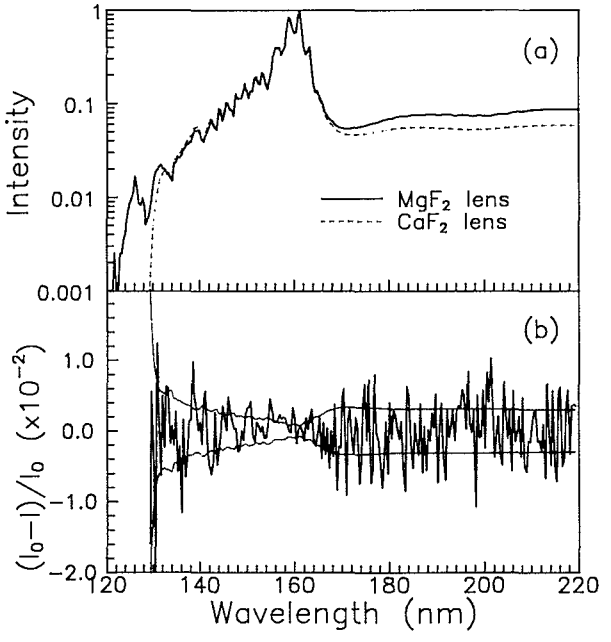

FIG. 2. (a) D_2 lamp spectral output and the short-wavelength cutoff for a MgF_2 vs a CaF_2 focusing lens. (b) Observed and calculated (statistical) noise spectrum for the response using a CaF_2 lens. Spectra were recorded at a slit resolution of 0.8 nm and a scan rate of 7.5 nm/min. Other parameters were: $1/\tau_{rep}=50$ Hz, $\tau_{gate}=800$ μs, $n_{pulse}=200$.

This error affects only relative intensities, which may be tolerable in instances where increased sensitivity is needed to detect weak features. In this work, we minimized counting error by operating at count rates C where $C\tau_{res}<0.10$ and typically <0.01. The major sources of noise affecting sensitivity are stray light, source fluctuations, and statistical counting noise. The statistical noise level $N(\lambda)$ per spectral point in an absorption spectrum is governed by the count rate $C(\lambda)$ and the counting duration t. The latter value is given by the product of the counting gate width τ_{gate} and the number of pulses summed per point n_{pulses}, leading to the expression

$$N(\lambda)=[C(\lambda)\cdot n_{pulses}\cdot\tau_{gate}]^{1/2}. \quad (1)$$

The broadband D_2-lamp response for typical scan conditions is plotted in Fig. 2(a). An instrument noise spectrum for absorption, measured by recording the signal $(I_0-I)/I_0$ in the absence of sample pulses, is given in Fig. 2(b). Comparison of the measured spectrum to a statistical noise spectrum calculated using Eq. (1) indicates that the major source of noise is statistical. Analog noise and lamp fluctuations effectively average to zero over the counting period t. Because of the long dead time between gas pulses, the I_0 gate is set to ten times the width of the I gate. This improves the counting statistics of I_0 by a factor of 3 and the overall signal/noise ratio for absorption measurements by about a factor of 2. This and other improvements in our apparatus since Fig. 2(b) was recorded allow us to detect absorptions as weak as $(I_0-I)/I_0\sim0.001$.

Absorption coefficient measurements. Ambient absorption spectra were recorded by filling the vacuum chamber used for free-jet experiments, which has a 30 cm path length, to pressures typically ranging from 20–60 mTorr (static sample). Absorption coefficients and cross sections were recorded at single wavelengths using a flowing sample. A hydrazine sample was contained in a bubbler and allowed to enter the chamber through a metering valve. The 10 ℓ chamber was pumped out at a rate of 10 ℓ/s giving about a 1 s sample residence time. Measurements were made at steady-state pressures ranging from 5 to 80 mTorr, corresponding to sample throughputs of 0.05–0.80 Torr ℓ/s.

Cross sections $\sigma(\text{cm}^2/\text{molecule})$ were determined from the expression

$$\frac{I}{I_0}=e^{-\sigma nl} \quad (2)$$

where $n(\text{molecule/cm}^3)$ is molecular density and $l(\text{cm})$ is path length. The commonly used absorption coefficient $k(\text{atm}^{-1}\,\text{cm}^{-1})$ is related to σ by $k=\sigma n_0$, where n_0 is molecular density at 1 atm.[34] It follows that

$$k=\frac{\ln(I_0/I)}{Pl}, \quad (3)$$

where $P(\text{atm})$ is pressure. Absolute pressures were measured using a baratron gauge.[35] I and I_0 were measured separately in the ambient sample experiments, corresponding to intensity in the presence and absence (evacuated) of sample, respectively.

There are two principle sources of uncertainty in the reported absorption coefficients. First, the potential exists for hydrazine decomposition on the chamber walls; however, we believe this to be a minimal problem due to passivation of all surfaces by the continuous flow of the sample. Second, a small leakage of chamber gas into the differentially pumped monochromator occurs through the windowless slit (100 $\mu\times4$ mm). Although the pressure rise in the monochromator is slight (1%–2% of the main chamber pressure), the path length is long (500 cm). Correction factors as large as 30% were determined from the measured pressure rise. The overall uncertainty in the absorption coefficients is estimated to be about $\pm20\%$. Our results are compared to other measurements[11,12,36,37] in Sec. III A.

Ionization measurements. Ionization is measured using a dual microchannel-plate detector (MCP). The voltage applied to the first surface is typically -2.2 kV, which creates a field of about 200 V/cm relative to the pulsed valve at ground potential. This is sufficient to draw the ions to the detector without external ion-optics components. The triple-pass reflector assembly was not used for the ionization experiments. Ion yields are measured by pulse counting. The MCP is operated near maximum gain (1 kV/plate) in order to approach gain-saturation conditions. The most common source of noise is ion feedback in the MCP due to electron-impact ionization of background gas in the channels. These readily identifiable noise bursts are avoided by reducing the ambient chamber pressure to about 1×10^{-5} Torr by employing mild expansion conditions (5 psi backing pressure, 10 Hz repetition rate). Jet-

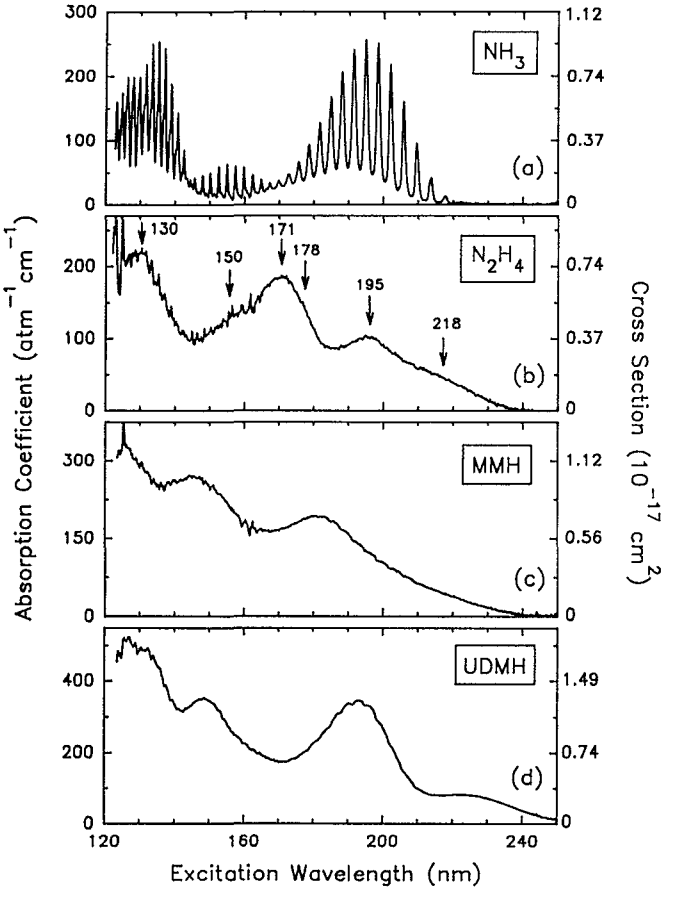

FIG. 3. Ambient absorption spectra of NH_3, N_2H_4, MMH, and UDMH recorded at a resolution of 0.4 nm and a scan rate of 6 nm/min. The arrows labelled by wavelength on the N_2H_4 spectrum refer to features that are discussed in the text.

cooled molecules and thermal-background molecules are ionized simultaneously by the light source. Ions were therefore counted over two gate periods; one that overlapped with the gas pulse and one that preceded it. The difference in intensity represents the yield of ions formed in the jet expansion. The pulse counts as a function of wavelength were normalized to the measured spectral response of the light source to derive ionization efficiency curves.

Sample preparation. Anhydrous-grade N_2H_4, MMH, and UDMH were obtained from Olin. The material was purified by freeze–thaw cycles using a cold bath slurry of liquid N_2 with CCl_4 (−23 °C) or $CHCl_3$ (−64 °C). A carrier gas of He or Ar was allowed to pass through a bubbler containing the sample and the resulting mixture flowed to the pulsed valve. The seed ratio was controlled by varying the carrier gas pressure and the bubbler bath temperature.

III. RESULTS

A. Absorption spectra

The uv/vuv absorption spectra of NH_3, N_2H_4, MMH, and UDMH are plotted in Fig. 3 to energies in excess of their first ionization potential. The NH_3 spectrum is dominated by long progressions of the ν_2 umbrella mode due to the change in geometry from a pyramidal ground state to planar excited states.[38–42] The measured absorption coefficients and cross sections depend on the instrumental bandwidth if it exceeds the natural linewidth. This is the case for the NH_3 lines at wavelengths shorter than 170 nm. The linewidths for the higher members of the $\tilde{A}$ state progression, on the other hand, are due largely to rapid predissociation and not instrumental broadening. We measured a peak absorption coefficient of 250 $atm^{-1}\,cm^{-1}$ ($\sigma_{max}=9.5\times10^{-18}$ cm^2) which is nearly identical to the value measured by Tannenbaum *et al.*[43,44] This value converts to an oscillator strength of 0.079,[43] which compares favorably to values reported by Watanabe (0.088)[45] and Harshberger (0.069).[46]

TABLE I. Comparison of hydrazine spectra to alkylamines, NH_3, and C_2H_4.

Molecule	R	Term values (eV)[a] I	II	III
H_2N–R	$-NH_2$[b]	4.22(w)[d]	2.66 (vs)	0.37 (vs)
		3.55 (m)		
		2.94 (w)		
	$-CH_3$[c]	3.87 (m)	2.57 (vs)	
$(CH_3)HN$–R	$-NH_2$[b]	(vw)	2.50 (vs)	0.77 (vs)
	$-CH_3$[c]	3.57 (w)	2.33 (vs)	
$(CH_3)_2N$–R	$-NH_2$[b]	3.35 (s)	2.39 (vs)	0.45 (vs)
	$-CH_3$[c]	3.03 (s)	2.30 (vs)	
NH_3[e]	$3a_1 \rightarrow 3sa_1'$, $\tilde{A}$ (4.44, vs); $3pe'$, $\tilde{B},\tilde{C}$ (2.83, m); $3de'$, $\tilde{D}$ (1.51, vs); $3da'$, $\tilde{D}''$ (1.47, m); $4sa_1'$, $\tilde{D}'$ (1.46, m); $4de'$, $\tilde{E}$ (0.84, vs)			
C_2H_4[f]	$1b_{1u}\rightarrow 3sa_g$ (3.41, vs); $3p\pi_y b_{2u}$ (2.68); $3p\pi_z b_{1u}$ (2.25); $3db_{1g}$, $3da_g$ (1.61)			

[a]Relative to the (n_+,∞) vIP at 9.91 eV. The (n_-,∞) vIP is 10.64 eV (Ref. 21).
[b]This work.
[c]References 49 and 50.
[d]Relative intensity.
[e]Reference 39.
[f]Reference 67.

The N_2H_4 absorption spectrum in Fig. 3(b) is broad at all wavelengths. The raw spectrum had a small component due to NH_3 impurity, which was subtracted away using a suitably scaled spectrum of pure NH_3. Some of the structure at short wavelength in Fig. 3(b) appears to be due to residual NH_3 signal. (The spectrum of N_2H_4 is the only one that required correction for impurity.)[47,48] Vacuum ultraviolet absorption spectra of N_2H_4 have been recorded by Schürgers and Welge,[13] by Biehl and Stuhl,[14] and by Lang.[36] All spectra are, in general, agreement, however, the present spectrum in Fig. 3(b) has better sensitivity and reveals weak features not apparent in the other spectra. (Also the spectra of Schürgers and Welge[13] and Lang[36] do not extend to the lowest energy features). The N_2H_4 absorption coefficients reported in Fig. 3 are about 15%–20% lower than that of Biehl and Stuhl and of Lang and about 30% lower than Schürgers and Welge. However, our values are about 50% larger than reported by Willis and Back for their 210–260 nm spectrum.[1] Finally, N_2D_4 has re-

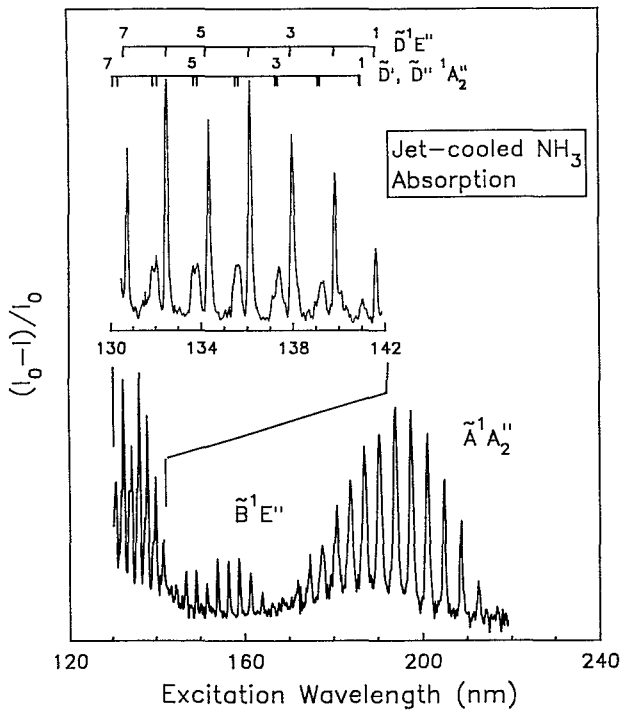

FIG. 4. Jet-cooled absorption spectra of NH_3. Resolution and scan rate were 0.5 nm and 3 nm/min for the bottom spectrum and 0.1 nm and 0.55 nm/min for the top spectrum (latter spectrum recorded for 10% NH_3 in He at 15 psi).

cently been reported[37] to have an absorption strength nearly twice as large as the above reported N_2H_4 spectra. Although a case can be made that a consensus is emerging centering around the values of Biehl and Stuhl, it is clear that considerable uncertainty still exists.

The absorption spectra of MMH and UDMH in Fig. 3 show similar broad features as N_2H_4 for all observed electronic bands. An increasing absorption strength is observed with methyl substitution. The change in band positions and intensities for the N_2H_4, MMH, and UDMH resemble the trends observed for the progression of spectra for monomethyl-, dimethyl-, and trimethylamine (these latter spectra were only recorded to a short wavelength limit of 160 nm).[49] The term values (i.e., excited-state ionization potentials) and relative intensities for these spectra are summarized in Table I.[44,49,50] A discussion of the excited electronic states of hydrazine is given in Sec. IV. The MMH and UDMH spectra by Lang[36] cover a narrower wavelength range than here, but the absorption strengths generally agree to within 10%–20% of our spectra.

Jet-cooled absorption spectra are presented in Figs. 4 and 5 for NH_3 and UDMH, respectively. The long ν_2 umbrella-mode progression of NH_3 is apparent in Fig. 4 even under low resolution (0.5 nm). At higher resolution (0.1 nm) the $\tilde{D}$ and $\tilde{D}'$, $\tilde{D}''$ states are clearly resolved. Individual bands of the nearly degenerate $\tilde{D}'$ and $\tilde{D}''$ states are resolvable at higher resolution. The single-photon absorption spectra benefit from supersonic cooling as evidenced by the greater resolution obtained here relative to previous spectra recorded by vuv excitation on ambient samples.[39,51–53] Single-photon absorption spectra of jet-cooled NH_3 have been previously reported for the $\tilde{A}$ state only.[38] High-resolution spectroscopy of the higher energy states has been measured by resonance multiphoton ionization.[39–41] However, some electronic states, such as the $\tilde{D}'$ and $\tilde{D}''$ are not observable due to rapid predissociation that competes with ionization.

The jet-cooled UDMH absorption spectrum in Fig. 5, unlike NH_3, does not show any resolvable vibrational structure at the experimental resolution of 0.2 nm, but instead resembles the spectrum under ambient conditions in Fig. 3. This comparison indicates that the continuous spectrum of UDMH is not due to thermal broadening, but to other factors such as large geometry changes or rapid dissociation. The former cause is the more likely explanation as discussed in Sec. IV. Because of the lower vapor pressures and weaker absorption strengths of N_2H_4 and MMH, we did not obtain absorption spectra of sufficient sensitivity to be useful.

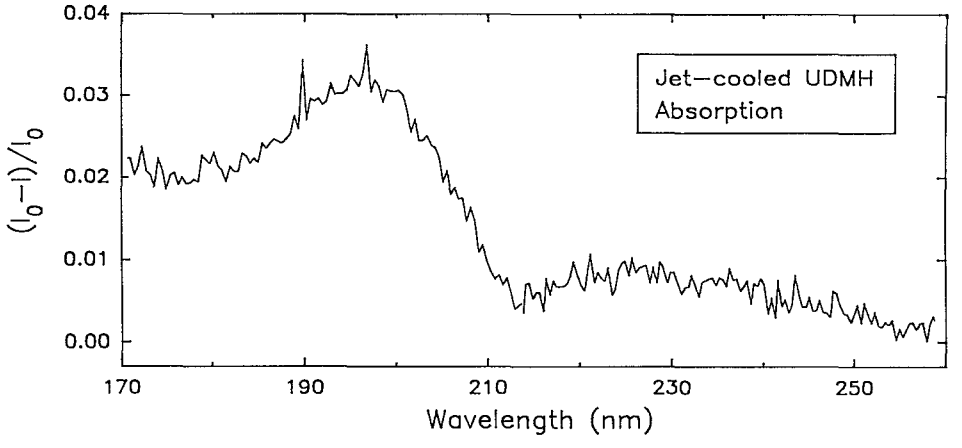

FIG. 5. Jet-cooled absorption spectrum of UDMH (10% in Ar at 8 psi) recorded at 0.2 nm slit resolution and a 6 nm/min scan rate.

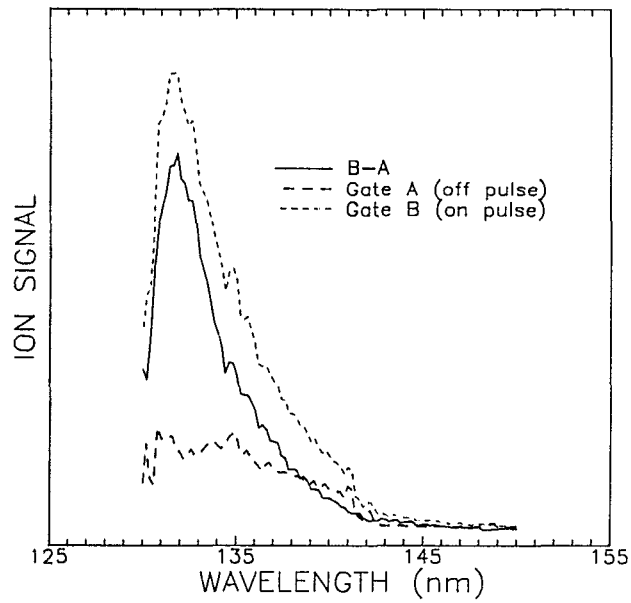

FIG. 6. Photoionization efficiency curves measured during pulsed valve on (gate B) and off periods (gate A). The difference in these signals (i.e., background subtraction) corresponds to the jet-cooled photoionization curve.

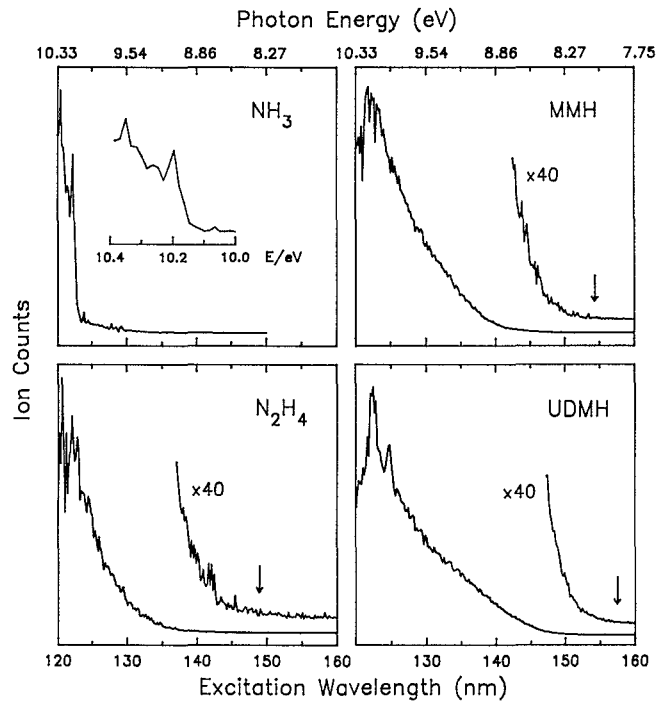

FIG. 7. Single-photon ionization efficiency curves for jet-cooled molecules. Resolution was 0.4 nm (0.03 eV at 120 nm) Other conditions are as follows: (NH_3) 10% in 6 psi He, 3 nm/min scan rate; (N_2H_4) 4% in 8 psi He, 3 nm/min scan rate; (MMH) 3% in 8 psi He; 1.2 nm/min scan rate; (UDMH) 10% in 8 psi He, 6 nm/min scan rate.

B. Ionization efficiency curves

Single-photon ionization efficiency curves are plotted in Figs. 6–8 for the four subject molecules under jet-cooled conditions. The long path length of the chamber (20 cm) relative to the jet (1 cm) creates a thermal-background ion signal that accounts for about 10% of the total signal. The jet-cooled and thermal ion signals are distinguishable by counting ions over two gate periods, one coincident with the gas pulse (gate B) and the other placed before or well after the gas pulse (gate A). Subtracting the thermal signal from the the total signal gives the jet-cooled spectrum as illustrated in Fig. 6. This procedure assumes that the background pressure is the same over the two gate periods.[54]

The ionization threshold of NH_3 has been studied extensively in the past by photoionization and photoelectron spectroscopy.[44,45,55–59] However, the adiabatic ionization potential has been difficult to establish because of the long Franck–Condon progression for ionization involving the ν_2 umbrella mode. The presumed 0,0 transition in the single-photon photoelectron spectrum is about 0.06 the intensity of the strongest peak at about $v=6$.[56] Also the Franck–Condon factor for the 0,1 hot band is much greater than for the 0,0 transition,[60] thus enhancing the former signal relative to the latter signal. Consequently, there is still some uncertainty whether the true origin is the more commonly assigned 0,0 transition at 10.18 eV or the tentative hot band at 10.07 eV. Calculations of Franck–Condon distributions disagree on the assignments; Ågren[61] favors an origin at 10.07 eV, while Botschwina[60] argues for 10.18 eV. (In principle, the distinction can be made at sufficiently high photoelectron resolution by determining whether the band separation is due to the ν_2 vibrational frequency of the neutral or the ion.) Although, the ionization potential is commonly accepted to be 10.18 eV, Locht *et al.* very recently made detailed measurements of photoionization steps and autoionization peaks for NH_3 and its isotopomers with deuterium and argues for the 10.07 eV origin.[59]

Our threshold-ionization measurement, free of hot-band structure, shows a distinct threshold at 10.16 ± 0.04 eV (Fig. 7). There is no discernable step at the expected energy of the 0,1 hot band other than a weak continuous

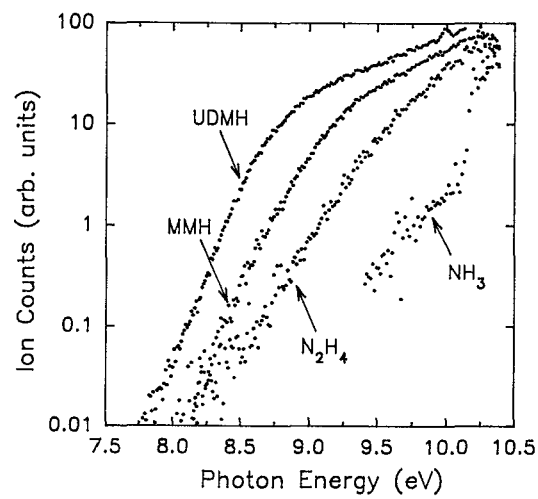

FIG. 8. The photoionization results of Fig. 7 plotted on a logarithmic scale to emphasize the threshold regions.

TABLE II. Comparison of ionization thresholds for NH_3 and hydrazine molecules.

Molecule	vIP[a]	aIP[c]	tIP[c]	ΔH_r[f]
NH_3	10.88	10.18	10.16	0.7
N_2H_4	9.95,9.91[b]	8.1,8.36[d]	8.32	1.7
MMH	9.35	7.7,7.67[d]	8.05	1.7
UDMH	8.85	7.29,7.46[d]	7.87	1.5

[a]Reference 32 and S. F. Nelsen, V. E. Peacock, and G. R. Weisman, J. Am. Chem. Soc. **98**, 5269 (1976); S. F. Nelsen and J. M. Buschek, *ibid.* **96**, 2392 (1974) unless otherwise noted.
[b]Reference 21.
[c]Reference 32 unless otherwise noted.
[d]M. E. Akopyan, F. I. Vilesov, and A. N. Terenin, Bull. Acad. Sci., USSR, Phys. Ser. **27**, 1504 (1963).
[e]This work.
[f]ΔH_r=vIP−aIP.

signal believed to be due to NH_3 clusters.[62] The 0,1 intensity in ambient NH_3 photoionization[44,45] and photoelectron spectra[56,57] is about 10% of the 0,0 intensity, which is much larger than that observed in Figs. 7 and 8. These observations support the assignment of the 10.07 eV feature to the 0,1 hot band and the 10.18 eV feature to the adiabatic ionization 0,0 transition. The two narrow (instrumental bandwidth limited) peaks at 10.20 and 10.35 eV are coincident with autoionization structure observed by Locht *et al.*[59] [We are tentative about assigning this structure, however, because the lamp output in this spectral region is weak and highly structured (Fig. 2), which can cause spurious residual peaks in the normalized ion signal.]

The ionization thresholds in Figs. 7 and 8 for the hydrazine compounds N_2H_4, MMH, and UDMH are much broader than the threshold for NH_3. This observation is consistent with an excitation involving a large geometry change. Other evidence includes the broad and featureless absorption spectra observed for hydrazines (Fig. 3) even under jet-cooled conditions (Fig. 5), and very large differences in the adiabatic and vertical ionization potentials (aIP and vIP, respectively) reported in previous work.[32,33] Values of vIP were determined from the peak positions in photoelectron spectra[21,30] whereas aIP were determined from charge–exchange equilibrium experiments[32] that allow for geometric relaxation. A compilation of these values are compared with the present threshold photoionization potentials (tIP) in Table II. Hydrazine cations (and presumably high-lying neutral electronic states) are planar;[26–29] therefore, ionization (and electronic-state excitation) involve substantial changes along coordinates that involve torsional and inversion modes. The geometries and their affect on electronic-state structure and energy is discussed below.

IV. DISCUSSION

A. General properties of hydrazine

Geometry plays a major role in explaining electronic and reactive properties of hydrazine. The more important geometric conformers for this discussion are represented in Fig. 9. The structures, corresponding to pyramidal nitrogen bonding, can interconvert by rotation about the N–N bond. Also the syn- and anticonformers can interconvert by an inversion at either nitrogen (NH_2 wag). The planar configuration is intermediate between syn and anti. The ground electronic state of N_2H_4 is believed to have pyramidal geometry (in analogy with NH_3) and to be rotated about 90° about the N–N bond in a staggered gauche orientation (C_2 symmetry) that minimizes the interaction between the lone-pair electrons.[15–23] Hence, the symmetric and antisymmetric combinations $n_\pm$ of the nitrogen nonbonding orbitals are nearly degenerate. This geometry is supported by *ab initio* calculations at various levels (SCF 4–31G, STO-3G, CNDO/2, MINDO/2)[15–21] and by photoelectron spectroscopy, the latter which shows a $n_+ - n_-$ splitting of 0.7 eV (vs 4–5 eV calculated for the syn and anti forms).[21] Calculated internal-rotation barriers vary from 9.6–13.7 and 1.6–6.2 kcal/mol at the syn- and anti-geometries, respectively.[15–17,20] The planar energy is not known except as far as the barrier to syn–anti-inversion is known; experimental[63] and theoretical[15,64] values range from 5–7.5 and 6.1–7.4 kcal/mol, respectively (NH_3 by comparison has a 5.8 kcal/mol barrier).[65]

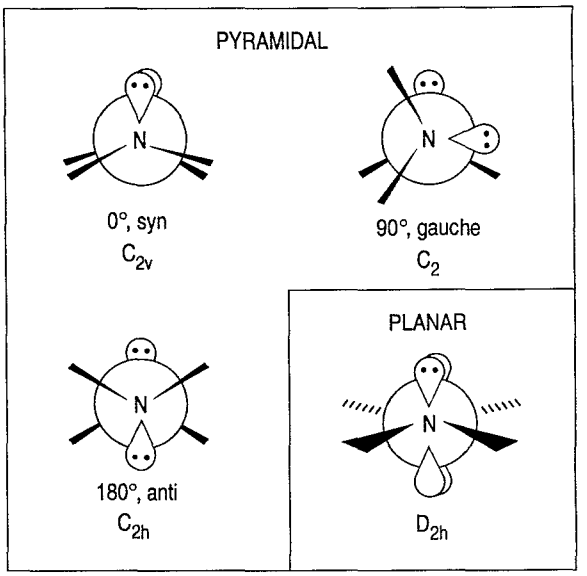

FIG. 9. Possible conformers of N_2H_4. The syn, *gauche*, and anticonformers can interconvert by rotation about the N–N bond. The syn and anti forms can also interconvert by inversion through the planar structure. The lone pair orbitals are sp^2 type for pyramidal nitrogen bonding and p type for planar nitrogen bonding.

The structure of hydrazine cation is reported to be planar at both nitrogen sites and planar overall (D_{2h} symmetry).[26–33] The evidence is based primarily on solution-phase measurements of the ESR hyperfine splitting $a(N)$ and the frequency and absorption strength of the (n_+,n_-) transition.[26–29] The ESR experiments are sensitive to the amount of s character in the nonbonded orbital, which apparently is small for $N_2H_4^+$ and other substituted hydrazine cations.[26–28] The optical experiments reveal strong absorption strengths and large splittings indicative of π–π^*

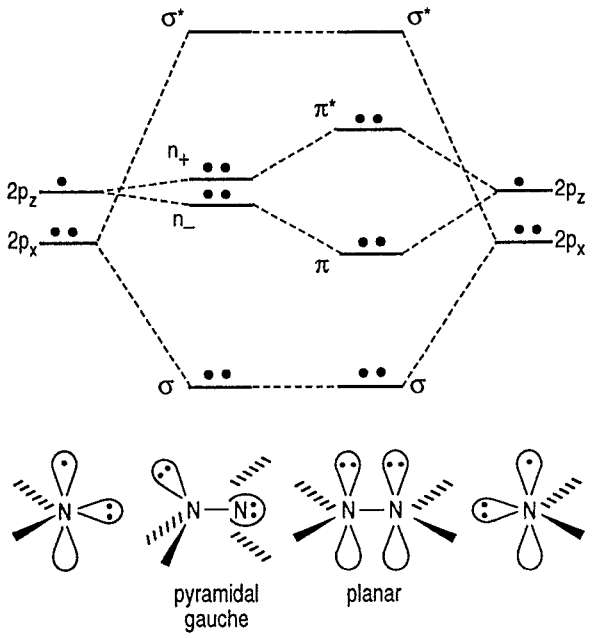

FIG. 10. Qualitative correlation diagram showing the interaction of NH_2 nonbonding orbitals for two different geometries of N_2H_4. The x axis is along the N–N bond and the z-axis is perpendicular to the molecular plane.

transitions.[26,29] Gas-phase experiments are consistent with a very large geometry change upon ionization. The vertical ionization potentials vIPs measured by photoelectron[21,30] and electron-impact spectroscopy[31] are much greater than the adiabatic ionization potentials aIPs determined from charge–transfer equilibrium studies.[32] The present photoionization measurements in Figs. 7 and 8 exhibit a broad Franck–Condon envelope with considerable spread between the threshold ionization energy (tIP$\geqslant$aIP) and the peak ionization energy (vIP) (Table II). The difference between vIP and aIP (measured[32] and calculated[33] to be 1.8 and 2.3 eV, respectively) represents the destabilization energy of the *gauche* conformer relative to the most stable ion geometry, presumed to be D_{2h} planar. In contrast, the conformers (Fig. 9) in the neutral ground electronic state all lie within about 0.5 eV of each other.

The unusually large change in structural stability upon hydrazine ionization can be understood by simple molecular-orbital arguments. A correlation diagram relating the nonbonding orbitals of fragment NH_2 to the orbitals of N_2H_4 is given in Fig. 10 for pyramidal *gauche* vs planar geometry. The axis system is for N_2H_4 where z is the rotation axis perpendicular to the N–N bond and x and y are, respectively, the long and short axes in the molecular plane. For simplicity, we represent the NH_2 nonbonding orbitals as p_z and p_x orbitals rather than hybrids involving s character (for planar approach, p_z is a good approximation). The lobe for p_x is highly idealized.[66] Nonetheless, this simple representation predicts the correct behavior and is therefore instructive.

The $2p_x$ orbitals of NH_2 overlap and interact strongly upon approach and split into N–N bonding and antibonding orbitals σ_{NN} and σ^*_{NN}.[66] The calculated splitting is $\geqslant$20 eV.[20] The interaction of two p_z orbitals depend strongly on the N–N rotation angle θ. Minimal interaction occurs for $\theta=90°$ (*gauche*) and hence the symmetric and antisymmetric combinations n_+ and n_-, respectively, are nearly degenerate (0.30 eV calculated splitting).[20] The calculated splitting as expected is much greater for $\theta=0°$ (syn, 4.30 eV) and $\theta=180°$ (anti, 5.30 eV).[20] Similarly, a strong interaction is expected for the planar geometry where the nonbonding orbitals are better described by π and π^* orbitals. We estimate the splitting to be $\geqslant$5.5 eV based on the $N_2H_4^+$ (π,π^*) absorption spectrum in solution.[29]

The geometry of neutral and ionic hydrazine can be predicted using the model in Fig. 10 by considering occupancy of molecular orbitals by the valence electrons. There are six valence electrons for the neutral molecule and five for the ion. For the six-electron case, the total electronic energy is not significantly different for the pyramidal *gauche* and planar geometries because the reduction in energy of the n_+ lone-pair electrons is offset by the increase in energy of the n_- lone-pair electrons. As a result, weaker effects such as steric interactions become important and explain in part the stability of the *gauche* conformer. The situation changes considerably for the five-electron ionic case. The removal of an electron now strongly favors the planar geometry because this allows two electrons to decrease in energy and only one to increase in energy. By this reasoning, the stabilization of planar relative to pyramidal *gauche* upon ionization is substantial, in accord with experimental observation.

Finally, we note that the simple model in Fig. 10 explains the behavior of ethylene electronic-state spectroscopy which has a similar MO construction as N_2H_4.[67–70] Because C_2H_4 has two fewer electrons than N_2H_4, the planar D_{2h} geometry is considerably more stable than the twisted form in the ground state. Excitation of an electron to a π^* orbital, however, makes the twisted D_{2d} form slightly more stable. Ionization or excitation to a Rydberg orbital, however, again favors the planar geometry, but not as strongly as in the ground state because only one electron is stabilized. The usefulness of the above simple picture encourages us to develop a more rigorous treatment of hydrazine molecular-orbital correlations in order to interpret the absorption and ionization spectra presented in Sec. III.

B. Electronic level structure

The N_2H_4 ground electronic-state configurations for 90° pyramidal *gauche* (C_2) and planar (D_{2h}) geometries (Fig. 9) are given by

$$[1a^2 1b^2]_{1sN}[2a^2]_{\sigma_{NN}}[2b^2 3a^2 3b^2 4a^2]_{\sigma_{NH}}[4b^2 5a^2]_{n_\pm}$$

$$C_2{:}\tilde{X}\,{}^1A,$$

$$[1a_g^2 1b_{3u}^2]_{1sN}[2a_g^2]_{\sigma_{NN}}[2b_{3u}^2 1b_{1g}^2 1b_{2u}^2 3a_g^2]_{\sigma_{NH}}[1b_{1u}^2 1b_{2g}^2]_{\pi_\pm}$$

$$D_{2h}{:}\tilde{X}\,{}^1A_g.$$

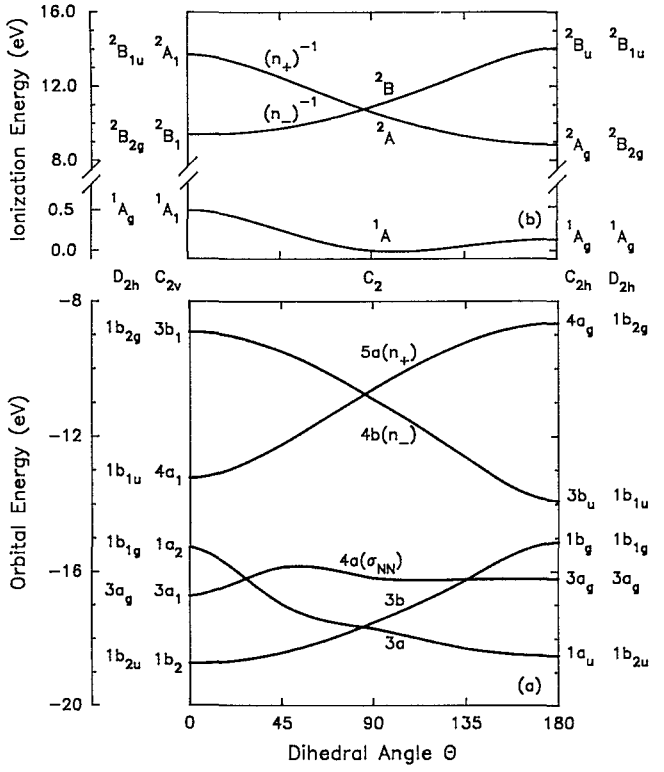

FIG. 11. (a) Molecular-orbital and (b) electronic-state energy dependence on θ for N_2H_4. A spline curve was fitted to the data of Fink *et al.* (Ref. 20) calculated for values of $\theta=0°$, 45°(−45), 90°, 135°(−135), 180°. Orbital energies represent molecular-orbital ionization potentials. Note that the energy scale varies for each plot. The D_{2h} symmetries for planar N_2H_4 are shown alongside the corresponding C_{2v} and C_{2h} elements.

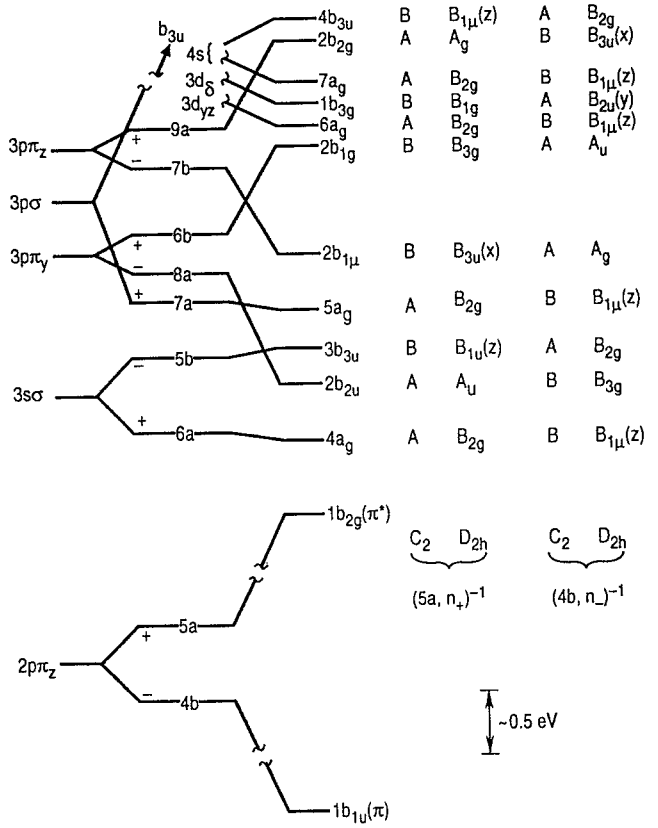

FIG. 12. Molecular-orbital correlation diagram for N_2H_4 singlet states of $C_2(90°)$ and $D_{2h}(180°)$ geometry constructed from symmetric and antisymmetric combinations of separated NH_2 orbitals. $n_+(5a)$ lies above $n_-(4b)$ for the presumed ground state angle $\theta=95°$; a reversal occurs at $\theta<85°$ (cf. Fig. 11). A similar ordering of the symmetric and antisymmetric orbitals for the $3p\pi_y$ and $3p\pi_z$ brackets is assumed for $\theta=95°$. The $3p\pi_y$ and $3p\pi_z$ orbitals are very similar in character and energy for C_2 90° *gauche*; however, we separate them for clarity and to better correspond to the energy ordering of the NH_2 and the N_2H_4 (D_{2h}) to which they correlate. A rough energy scale is indicated based on the calculated C_2H_4 orbital energies (note the breaks in the scale for the $2p\pi_{z\pm}$ correlations).

The sequence of orbitals for C_2 are in order of calculated energies.[20] The energy ordering changes in going to D_{2h}; however, we list these orbitals in the same order as the C_2 elements to show the symmetry correspondences. The bond designations are only approximate (e.g., $[2a_g^2]_{\sigma NN}$ and $[3a_g^2]_{\sigma NH}$ are probably mixed). Orbital energies calculated by Fink *et al.*[20] are plotted as a function of θ in Fig. 11. Symmetry designations are shown for C_{2v} (syn, $\theta=0°$), C_2 ($0<\theta<180°$), and C_{2h} (anti, $\theta=180°$). D_{2h} symmetry is obtained by flattening either the syn- or antigeometries and the corresponding symmetry designations are labeled alongside the C_{2v} and C_{2h} labels. We are not aware of any reported orbital energies of N_2H_4 for D_{2h}. The $5a(n_+)$ and $4b(n_-)$ energies are strongly dependent on the dihedral angle θ about the N–N bond. ($5a$ is slightly higher in energy at $\theta=90°$ and at the presumed ground state angle of $\theta\simeq95°$.)

Fink *et al.* also calculated total energy (kinetic energy and nuclear–nuclear, nuclear–electron, and electron–electron repulsion) from which they derived a ground state potential along the rotation coordinate θ [Fig. 11(b)].[20] The quality of these results can be judged by comparing their calculated barrier to internal rotation at the syn- and anticonfigurations of 11.31 and 3.12 kcal/mol, respectively, to the range of values calculated by other investigators (9.6–13.7 and 1.6–4.6 kcal/mol, respectively).[15,16] Their orbital energies are also in good agreement with other data calculated at the minimum energy geometry $\theta\simeq90°$–100°.[17,18] We computed ionic-state potentials in Fig. 11(b) for ionization of an electron from either n_+ or n_- by subtracting the appropriate orbital energy from the ground state potential (Koopman's assumption[71]). This exercise corroborates that a large geometry change occurs upon ionization. The calculated vIP and aIP for a C_{2h} ion is 10.7 and 8.8 eV, respectively, which is comparable to experimental values of 9.95 and 8.2 eV (Table II). Unfortunately, comprehensive calculations are not available for D_{2h} geometry; however, Peel has calculated values of vIP and aIP of 9.8 and 7.5 eV assuming a C_2 to D_{2h} ionization.[33]

The current state of theory is insufficient for interpreting electronic-state spectra of hydrazines. There is virtually no data available on the energies of the occupied orbitals for D_{2h} symmetry nor are energies for higher-lying unoccupied orbitals known for any symmetry. All that exists is a C_2 calculation for the $3s$ orbitals by Staemmler[24] and

some orbital correlations for bond breaking by Evleth.[25] The planar D_{2h} geometry is expected to be stable for many excited electronic states (particularly Rydberg states) and knowledge of high-lying MO energies would allow estimates of transition energies. We have developed an approximate molecular-orbital (MO) diagram for N_2H_4 in Fig. 12 starting from a framework based on orbital energies of C_2H_4 in D_{2h} geometries.[67–70] A variety of assumptions and guiding principles were used to estimate the level structure for N_2H_4 in C_2 and D_{2h}. Our intent in constructing the orbital diagram in Fig. 12 is to obtain a qualitatively correct ordering of N_2H_4 singlet excited-state orbitals for C_2 and D_{2h} geometry and an understanding of the relative dependence of energy on geometry.

The calculated MOs of C_2H_4 (Ref. 68) are a good basis to start with, given the fact that the lower occupied MOs have the same order of energy as that calculated for C_{2v} and C_{2h} hydrazine when expressed as planar D_{2h} symmetry elements (Fig. 11). According to Mulliken, because the occupied MOs are precursors to the Rydberg MOs, the latter should follow closely the symmetry ordering of the former.[67] We, therefore, expect a close association in the order of excited-state MOs of N_2H_4 and C_2H_4 in planar D_{2h} geometry. The excited-state ordering of N_2H_4 in C_2 *gauche* geometry is determined by finding a sequence of orbitals that (1) correlates with the D_{2h} orbitals, (2) represents symmetric and antisymmetric combinations of fragment NH_2 orbitals, and (3) shows splittings and dependences on geometry that are consistent with orbital-overlap arguments. We discuss below each bracket (i.e., symmetric/antisymmetric combination) originating from the NH_2 orbitals below.

The calculated splitting of the $3s\sigma$ bracket is similar for $C_2H_4(D_{2h})$ (Ref. 68) and $N_2H_4(C_2)$ (Ref. 24) (0.6–0.7 eV) indicating that rotation about θ and inversion about nitrogen have minor affects on the $3s$–$3s$ overlap. The strongest $3p$ interaction, based on orbital overlap considerations, is expected to be the $3p\sigma \pm 3p\sigma$ combination. Indeed, a large splitting is calculated for $C_2H_4(D_{2h})$.[68] Because these orbitals are symmetric about the N–N bond, we expect only moderate energy dependence on bond rotation and pyramidization and, therefore, assume that $7a$ is similar in energy to the corresponding $5a_g$ orbital. (We ignore the dependence of the relative energy on changes in the N–N bond length). The $3p\pi_z \pm 3p\pi_z$ and $3p\pi_y \pm 3p\pi_y$ combinations will have maximum and minimum overlap for $\theta=0°$ D_{2h} and $\theta=90°$ C_2 rotation, respectively. The calculated splittings for $C_2H_4(D_{2h})$ are about 1 eV for both sets of p orbitals.[68] We assume minimal splittings in Fig. 12 for $\theta=90°$ C_2 (certainly they must be less than the more localized $2p\pi_z$ splitting).

C. Assignment of hydrazine electronic-state spectra

Excited-state symmetries are given in Fig. 12 for C_2 and D_{2h} geometries for electron excitation originating from the n_+ and n_- orbitals. The $(n_-)^{-1}$ excitations are analogous to ethylenic transitions in D_{2h}. All of the singlet excited states are dipole allowed for $C_2 \rightarrow C_2$ transitions since ^1A state excitation corresponds to a z-component transition dipole and ^1B state excitation corresponds to x,y-component transition dipoles. The $D_{2h} \rightarrow D_{2h}$ dipole-allowed states are $^1B_{1u}(z)$, $^1B_{2u}(y)$, and $^1B_{3u}(x)$. The selection rules for $C_2 \rightarrow D_{2h}$ states will be mixed between the cases described above. These transitions should be viewed as excitation to vibrationally excited D_{2h} states and, therefore, have large Franck–Condon distributions as discussed earlier.

The correlation diagram in Fig. 12 is useful for assigning the spectra in Fig. 3, although a definitive explanation is not yet possible. (This should not be surprising given the many conflicts and uncertainties that still exist for the extensively studied spectroscopy of C_2H_4.)[67–70] It seems reasonable to try to assign the hydrazine spectra by finding features that resemble either ethylenic-type absorptions or substituted ammonia-type absorptions. In fact, the spectra for N_2H_4, MMH, and UDMH bear strong resemblances to the spectra of monomethyl-, dimethyl-, and trimethylamine, respectively (these latter spectra were recorded only for $\lambda > 160$ nm).[44,49,50] Both series of molecules are of the form RNH_2, $RNH(CH_3)$, and $RN(CH_3)_2$, where R $=NH_2$ or CH_3. The term values and relative intensities for the most discernable bands are summarized in Table I. Weaker bands are evident for the hydrazine spectra as shoulders on the larger bands in Fig. 3.

All transitions for NH_3, methylated ammonia, and the hydrazines involve promotion of a lone-pair electron from a nonbonding $2p$-type orbital to Rydberg-type orbitals and so spectral similarities might be expected for these molecules. The hydrazines are more complicated because of the symmetric and antisymmetric combinations of the NH_3-type orbitals, which open up additional excitations (e.g., ethyleniclike transitions, Fig. 12). Given the similarities of the hydrazine spectra to the methylamine spectra (Table I), it seems reasonable to assign bands I and II of hydrazine to $3s$ and $3p$ excitations in accordance with the methylamine assignments. These assignments are consistent with the magnitude of the term values for NH_3 and the expected shifts due to methylation.[44] The strong hydrazine band III may be attributed to $4d$ excitation. A difficulty to the methylamine assignments, however, is that aside from the term values, they do not compare well to NH_3 in two major respects: first, the $3p$ transitions, which are formally forbidden and weak in NH_3, are very prominent in the methylamines, and second, the $3d$ transitions, which are strong in NH_3, are nearly absent in the methylamines. It is tempting to reassign the $3p$ transition as a $3d$ transition, however, then the term value would be inconsistent with a $3d$ orbital (cf. NH_3 and C_2H_4 in Table I). The different behavior for alkylamines compared to NH_3, however, has been recognized and rationalized in the past.[50] For example, the term value for the $(n,3s)$ transition decreases much more rapidly with methylation than do the $(n,3p)$ transitions, which is expected based on the usually stronger interaction of substituents with s orbitals than p orbitals. The reversal in the relative intensity of $3s$ and $3p$ excitation in alkylamines vs NH_3 seems to be a general feature for symmetric alkylation and is also observed for ketones, sulfides, and azoalkanes.[50] Finally, the anomalously weak $(n,3s)$

transition for dimethylamine (and likewise for the disubstituted amine, MMH) is also observed for larger dialkylamines.

The orbital diagram in Fig. 12 enables us to determine the likely transitions contributing to the hydrazine electronic-state absorption spectra in Fig. 3. Glownia *et al.* found that NH_3 absorption spectra could be largely explained by D_{3h} selection rules even though the ground state has pyramidal C_{3v} symmetry.[39] We should, likewise, expect the hydrazine spectra to roughly follow D_{2h} selection rules (assuming the excited states are planar). The excited-state designations are based on the correlation from C_2 (90°, pyramidal) to C_{2h} (180°, pyramidal) to D_{2h} (180°, planar) geometry.

There are two dipole-allowed $3s$ transitions corresponding to $^1B_{1u}(n_-,3s\sigma_+)$ and $^1B_{1u}(n_+,3s\sigma_-)$. They occur at similar energy based on a separation given by the difference of the $2p\pi_{z\pm}$ splitting (0.7 eV measured[21]) and the $3s\sigma_\pm$ splitting (also 0.7 eV calculated[24]). We assign these transitions to the 195 nm band in Fig. 3(b). There are two other $3s$ transitions to states labeled $^1B_{2g}(n_+,3s\sigma_+)$ and $^1B_{2g}(n_-,3s\sigma_-)$ that lie about 0.7 eV below and above, respectively, the B_{1u} states. Staemmler calculated vertical $C_2 \rightarrow C_2$ energies and oscillator strengths for the four $n \rightarrow 3s$ excitation and finds $^1B_{2g}(n_+,3s\sigma_+)$ and $^1B_{2g}(n_-,3s\sigma_-)$ to be the weakest and second strongest transitions, respectively. It is reasonable to assign these transitions to the 218 and 178 nm bands, respectively. If these assignments are correct, then according to Table I, the term values for $^1B_{2g}(n_+,3s\sigma_+)$ and $^1B_{1u}(n_+,3s\sigma_-)$ are about 4.2 and 3.6 eV, respectively, and the values for $^1B_{1u}(n_-,3s\sigma_+)$ and $^1B_{2g}(n_-,3s\sigma_-)$ are about 3.6 and 3.0 eV, respectively, [4.2 and 3.6 eV relative to the (n_-,∞) ionization threshold].[72]

The next series of excitations are due to $n \rightarrow 3p$ transitions. Unfortunately, no calculations have been reported for electronic states above the $3s$ level, therefore, we resort to identifying D_{2h} selection rules. This assumption may improve for the higher Rydberg states since they are less likely to have valence character that might reduce the stability of the planar geometry. There are four D_{2h} dipole-allowed excited states for $n \rightarrow 3p$ excitation (Fig. 12). The $^1B_{1u}(n_-,3p\sigma_+)$ and $^1B_{3u}(n_+,3p\pi_{z-})$ states are estimated to have term values of about 2.5 eV. These coincide well with the 171 nm band in Fig. 3(b) (band II in Table I). The $^1B_{3u}(n_-,3p\pi_{z+})$ should lie roughly 0.6–1.0 eV to higher energy and the $^1B_{1u}(n_+,3p\sigma_-)$ state to somewhat higher energy. These transitions may explain the apparent shoulder to the high-energy side of the 171 nm band in Fig. 3(b).

The low-lying $n \rightarrow 3d$ and $n \rightarrow 4s$ transitions are expected to have excitation energies similar to the high-lying $n \rightarrow 3p$ transitions. According to Fig. 12, one expects the following D_{2h} dipole-allowed states to have term values in the vicinity of 1.5–2.0 eV: $^1B_{1u}(n_+,3p\sigma_-)$, $^1B_{1u}(n_+,4s\sigma_-)$, $^1B_{1u}(n_-,3d\delta_{\cos+})$, $^1B_{2u}(n_-,3\,d\delta_{\sin+})$, and $^1B_{1u}(n_-,4s\sigma_+)$. The $3d$ state descriptions are from Mulliken's assignment of C_2H_4.[67] Finally, we can only surmise that the strong bands labeled III in Table I [e.g., 130 nm band of N_2H_4 in Fig. 3(b)] with term values of about 0.5 eV are due to $n \rightarrow 4d$ transitions.

There are unresolved issues regarding the nature of the photoexcited geometry changes that could alter the above interpretation or require a more complex description. For instance, we consider only the 90°→180° correlations, although promotion of an n_- electron most surely favors a 90°→0° correlation to minimize energy. This causes a reversal in the symmetry designations for some of the symmetric/antisymmetric orbitals, however, it does not appear to change the D_{2h} selection rules and assignments presented above.

It is interesting to speculate on the C_2–D_{2h} structural relaxation energy ΔH_r for the excited states. The strong stabilization of the D_{2h} geometry due to promotion of a nonbonding electron (ion core case) assures that all excited states will be stable in this geometry. The value of ΔH_r for the excited states, however, will vary depending on the difference in the excited-state orbital energies for C_2 and D_{2h} geometries. This difference appears significant for the symmetric(+) and antisymmetric(−) combinations of the $3p\pi_{y\pm}$ and $3p\pi_{z\pm}$ orbitals according to Fig. 12. It is predicted that the (+,+) and (−,−) transitions will decrease ΔH_r relative to the ion core value of 1.7 eV, and that the cross transitions (+,−) and (−,+) will increase ΔH_r by a similar amount. Analysis of band shapes should provide some information on these possible effects.

V. SUMMARY AND CONCLUSION

We have presented single-photon vuv absorption and ionization spectra of ambient and jet-cooled NH_3, N_2H_4, MMH, and UDMH. The photoionization efficiency curve for jet-cooled NH_3 is consistent with the assignment of the 10.18 eV ionization threshold to the adiabatic 0,0 transition and the 10.07 eV threshold observed in previous ambient NH_3 photoionization and photoelectron spectra to the 0,1 hot band. The photoionization efficiency curves for the hydrazines exhibit broad thresholds indicating a very large geometry change upon ionization. The most stable geometries of N_2H_4 are purported to be C_2 *gauche* in the ground state neutral molecule and D_{2h} planar in the ground state ion. The absorption spectra of the hydrazines also show broad bands. A course assignment of the hydrazine spectra was first made by noting strong similarities to reported methylamine spectra. A molecular-orbital diagram correlating relative energies and symmetries of C_2 and D_{2h} orbitals was then constructed to identify and assign specific transitions to the observed bands and to better understand the dependence of each excited-state orbital on geometry. Although a pyramidal to planar bond reorganization about the nitrogen atoms occurs in analogy to NH_3, a large part of the structural reorganization energy ΔH_r is due to a 90° N–N bond rotation. Promotion of an electron from a nonbonding orbital causes the molecule to rotate from a position of minimum orbital overlap to a position of maximum overlap.

The dynamics of photo-rearrangement are not well understood. The energy diagram in Fig. 11 predicts that the direction of internal rotation depends on which nonbonded

electron is excited. For example, $(n_-)^{-1}$ ionization (^2B excitation) brings about rotation toward $\theta=0°$, whereas $(n_+)^{-1}$ ionization (^2A excitation) causes a rotation toward $\theta=180°$. However, if planarization of the pyramidal nitrogen bonds occurs first, then both rotations are equivalent (i.e., $D_{2d}\rightarrow D_{2h}$). In any case, the ^2A and ^2B states of C_2 symmetry undergo a barrierless conversion to a single $^2B_{2g}$ state of D_{2h} symmetry. The strong D_{2h} stability of the $N_2H_4^+$ ion core assures that all neutral Rydberg-type states will also be stable in D_{2h}. However, the value of ΔH_r will vary depending on the difference in the excited-state orbital energies for C_2 and D_{2h}. The effect should be strongest for low-lying y- and z-component Rydberg states (e.g., $3p\pi_{y\pm}$ and $3p\pi_{z\pm}$) and diminish for higher Rydberg states as the excited electron becomes less coupled to the molecular framework.

A better understanding of the spectroscopy and dynamics of hydrazines is currently hampered by insufficient knowledge of hydrazine molecular orbitals for relevant geometries. We have attempted to gain some understanding of the excited-state orbitals by drawing correlations to the separated fragment orbitals of NH_2 and by comparing energy ordering to the extensively studied case of ethylene. It would be useful to have calculations of the occupied orbitals for D_{2h} symmetry and calculations of the higher unoccupied orbitals for all symmetries considered here.

ACKNOWLEDGMENTS

We are grateful to R. A. Hertz for discussions involving preliminary calculations of hydrazine molecular orbitals. We thank Dr. V. I. Lang for making her hydrazine spectra available to us before publication. This work was funded by the Aerospace Sponsored Research program.

[1] C. Willis and R. A. Back, Can. J. Chem. **51**, 3605 (1973).
[2] D. A. Ramsey, J. Phys. Chem. **57**, 415 (1953).
[3] G. S. Chandler and A. D. McLean, J. Chem. Phys. **71**, 2175 (1979).
[4] P. Lindberg, D. Raybone, J. A. Salthouse, T. M. Watkinson, and J. C. Whitehead, Mol. Phys. **62**, 1297 (1987).
[5] W. G. Hawkins and P. L. Houston, J. Phys. Chem. **86**, 704 (1982).
[6] M. Arvis, C. Devillers, M. Gillois, and M. Curtat, J. Phys. Chem. **78**, 1356 (1974).
[7] K. H. Becker and K. D. Bayes, J. Phys. Chem. **71**, 371 (1967).
[8] F. E. Logan and J. M. Marchello, J. Chem. Phys. **49**, 3929 (1968).
[9] M. Gehring, K. Hoyermann, H. Schacke, and J. Wolfrum, *14th Symposium (Int.) on Combustion* (The Combustion Institute, Pittsburgh, 1972), p. 99.
[10] S. N. Foner and R. L. Hudson, J. Chem. Phys. **49**, 3724 (1968); **53**, 4377 (1970).
[11] E. W. Fournier, J. Steadman, R. A. Hertz, and J. A. Syage, Appl. Spectrosc. **45**, 468 (1991).
[12] J. A. Syage, J. Chem. Phys. **97**, 6085 (1992).
[13] M. Schürgers and K. H. Welge, Z. Naturforsch. Teil A **23**, 1508 (1968).
[14] H. Biehl and F. Stuhl, J. Photochem. Photobiol. A **59**, 135 (1991).
[15] J. O. Jarvie and A. Rauk, Can. J. Chem. **52**, 2785 (1974); J. O. Jarvie, A. Rauk, and C. Edmiston *ibid.* **52**, 2778 (1974).
[16] L. Radom, W. J. Hehre, and J. A. Pople, J. Am. Chem. Soc. **94**, 2371 (1972); L. Pedersen and K. Morokuma, J. Chem. Phys. **46**, 3941 (1967); E. C. Wagner, Theor. Chim. Acta **23**, 115 (1971).
[17] A. C. Hopkinson and M. H. Lien, Int. J. Quantum Chem. **13**, 349 (1978).
[18] M. M. Heaton, J. Am. Chem. Soc. **100**, 2004 (1978).
[19] A. H. Cowley, D. J. Mitchell, M.-H. Whangbo, and S. Wolfe, J. Am. Chem. Soc. **101**, 5224 (1979).
[20] W. H. Fink, D. C. Pan, and L. C. Allen, J. Chem. Phys. **47**, 895 (1967).
[21] K. Osafune, S. Katsumata, and K. Kimura, Chem. Phys. Lett. **19**, 369 (1973).
[22] J. R. Durig, S. F. Bush, and E. E. Mercer, J. Chem. Phys. **44**, 4238 (1966); J. R. Durig and W. C. Harris, *ibid.* **51**, 4457 (1969); Y. Hamada, A. Y. Hirakawa, K. Tamagake, and M. Tsuboi, J. Mol. Spectrosc. **35**, 420 (1970).
[23] N. Ohashi, W. J. Lafferty, and W. B. Olson, J. Mol. Spectrosc. **117**, 119 (1986); N. Ohashi and J. T. Hougen, *ibid.* **112**, 384 (1985); N. Tanaka, Y. Hamada, Y. Sugawara, M. Tsuboi, S. Kato, and K. Morokuma, J. Mol. Spectrosc. **99**, 245 (1983).
[24] V. Staemmler, Acta Phys. Pol. A **74**, 331 (1988).
[25] E. M. Evleth, Chem. Phys. Lett. **38**, 516 (1976); E. M. Evleth and E. Kassab, J. Am. Chem. Soc. **100**, 7859 (1978).
[26] S. F. Nelsen, S. C. Blackstock, N. P. Yumibe, T. B. Frigo, J. E. Carpenter, and Frank Weinhold, J. Am. Chem. Soc. **107**, 143 (1985).
[27] S. F. Nelsen, Acc. Chem. Res. **14**, 131 (1981).
[28] S. F. Nelsen, G. R. Weisman, P. J. Hintz, D. Olp, and M. R. Fahey, J. Am. Chem. Soc. **96**, 2196 (1974).
[29] E. Hayon and M. Simic, J. Am. Chem. Soc. **94**, 42 (1972).
[30] N. Bodor, M. J. S. Dewar, W. B. Jennings, and S. D. Worley, Tetrahedron **26**, 4109 (1970); S. F. Nelsen and J. M. Buschek, J. Am. Chem. Soc. **96**, 2392 (1974).
[31] V. H. Dibeler, J. L. Franklin, and R. M. Reese, J. Am. Chem. Soc. **81**, 68 (1959).
[32] S. F. Nelsen, M. R. Willi, and T. B. Frigo, J. Am. Chem. Soc. **106**, 7384 (1984); S. F. Nelsen, D. T. Rumack, and M. Meot-Ner (Mautner), *ibid.* **110**, 7945 (1988); M. Meot-Ner (Mautner).
[33] J. B. Peel, Aust. J. Chem. **39**, 1281 (1986).
[34] Another common measure of absorption strength is the extinction coefficient $\epsilon(1\ \text{mol}^{-1}\ \text{cm}^{-1})$ given by $\epsilon=A\cdot RT/V$.
[35] J. F. O'Hanlon, *A User's Guide to Vacuum Technology* (Wiley, New York, 1980).
[36] V. I. Lang (to be submitted).
[37] A. Hopkirk, J. A. Salthouse, R. W. P. White, J. C. Whitehead, and F. Winterbottom, Chem. Phys. Lett. **188**, 399 (1992).
[38] V. Vaida, W. Hess, and J. L. Roebber, J. Phys. Chem. **88**, 3397 (1984); V. Vaida, M. I. McCarthy, P. C. Engelking, P. Rosmus, H. J. Werner, and P. Botschwina, J. Chem. Phys. **86**, 6669 (1987).
[39] J. H. Glownia, S. J. Riley, S. D. Colson, and G. C. Nieman, J. Chem. Phys. **73**, 4296 (1980).
[40] J. H. Glownia, S. J. Riley, S. D. Colson, and G. C. Nieman, J. Chem. Phys. **72**, 5998 (1980); J. H. Glownia, S. J. Riley, S. D. Colson, J. C. Miller, and R. N. Compton, *ibid.* **77**, 68 (1982); J. B. Pallix and S. D. Colson, J. Phys. Chem. **90**, 1499 (1986).
[41] M. N. R. Ashfold, R. N. Dixon, N. Little, R. J. Stickland, and C. M. Western, J. Chem. Phys. **89**, 1754 (1988); M. N. R. Ashfold, R. N. Dixon, K. N. Rosser, R. J. Stickland, and C. M. Western, Chem. Phys. **101**, 467 (1986); M. N. R. Ashfold, R. N. Dixon, and R. J. Stickland, *ibid.* **88**, 463 (1984).
[42] A. E. Douglas and J. M. Hollas, Can. J. Chem. **39**, 479 (1961).
[43] E. Tannenbaum, E. M. Coffin, and A. J. Harrison, J. Chem. Phys. **21**, 311 (1953).
[44] M. B. Robin, *Higher Excited States of Polyatomic Molecules*, Vol. I (Academic, New York, 1974), p. 208 ff.
[45] K. Watanabe and J. R. Mottl, J. Chem. Phys. **26**, 1773 (1957); K. Watanabe, *ibid.* **22**, 1564 (1954).
[46] W. R. Harshbarger, A. Skerbele, and E. N. Lassettre, J. Chem. Phys. **54**, 3784 (1971).
[47] Willis and Back (Ref. 1) also observed a difficult to remove NH_3 impurity that they subtracted from their absorption spectrum. They argue that the structure reported in early spectra of N_2H_4 (Ref. 48) is due to NH_3 or other impurities.
[48] S. Imanishi, Nature (London) **127**, 782 (1931); S. Imanishi, Sci Pap. Inst. Phys. Chem. Res. **15**, 166 (1931); H. J. Hilgendorff, Z. Phys. **95**, 781 (1935).
[49] E. Tannenbaum, E. M. Coffin, and A. J. Harrison, J. Chem. Phys. **21**, 311 (1953).

[50] A. B. Cornford, D. C. Frost, F. G. Herring, and C. A. McDowell, Can. J. Chem. **49**, 1135 (1971).
[51] A. M. Quinton and J. P. Simon, J. Chem. Soc. Faraday Trans. 2 **78**, 1261 (1982); H. Okabe and M. Lenzi, J. Chem. Phys. **47**, 5241 (1967).
[52] M. Suto and L. C. Lee, J. Chem. Phys. **78**, 4515 (1983).
[53] M. Furlan, M.-J. Hubin-Franskin, J. Delwiche, D. Roy, and J. E. Collin, J. Chem. Phys. **82**, 1797 (1985).
[54] The thermal background does not increase until after the gas pulse has collided with the chamber walls, which occurs about 1 ms after the gas pulse firing. Therefore, the background signal is fairly constant just before and during the gas pulse period.
[55] J. Berkowitz, *Photoabsorption, Photoionization, and Photoelectron Spectroscopy* (Academic, New York, 1979), pp. 125–30, 265–71.
[56] J. W. Rabalais, L. Karlsson, L. O. Werme, T. Bergmark, and K. Siegbahn, J. Chem. Phys. **58**, 3370 (1973).
[57] M. J. Weiss and G. M. Lawrence, J. Chem. Phys. **53**, 214 (1970); G. R. Branton, D. C. Frost, F. G. Herring, C. A. McDowell, and I. A. Stenhouse, Chem. Phys. Lett. **3**, 581 (1969); A. W. Potts and W. C. Price, Proc. R. Soc. London Ser. A **326**, 181 (1972).
[58] T. J. Xia, T. S. Chien, C. Y. Robert Wu, and D. L. Judge, J. Quantum Spectrosc. Radiat. Trans. **45**, 77 (1991); V. H. Dibeler, J. A. Walker, and H. M. Rosenstock, J. Res. Natl. Bur. Stand. A **70**, 459 (1966).
[59] R. Locht, B. Leyh, W. Denzer, G. Hagenow, and H. Baumgärtel, Chem. Phys. **155**, 407 (1991).
[60] P. Botschwina, in *Ion and Cluster Ion Spectroscopy and Structure*, edited by J. P. Maier (Elsevier, New York, 1989) p. 59.
[61] H. Ågren, I. Reineck, H. Veenhizen, R. Maripuu, R. Arneberg, and L. Karlsson, Mol. Phys. **45**, 477 (1982).
[62] The slowly rising signal below threshold may be due to ammonia clusters and/or impurity (e.g., hydrazines); in either case it is a minor contribution. Clustering was minimized by using a sonic nozzle (i.e., not conical) heated to about 60 °C and operating under mild expansion conditions.
[63] Y. Hamada, A. Y. Hirakawa, K. Tamagake, and M. Tsuboi, J. Mol. Spectrosc. **35**, 420 (1970); M. D. Harmony and P. A. Baron, J. Mol. Struct. **38**, 1 (1977).
[64] A. Rauk, J. D. Andose, W. G. Frick, R. Tange, and K. Mislow, J. Am. Chem. Soc. **93**, 6507 (1971).
[65] J. D. Swalen and J. A. Ibers, J. Chem. Phys. **36**, 1914 (1962).
[66] For sp^2 hybridization, two N p orbitals are involved in σ-like N–H bonding and the other is nonbonding. The latter higher energy orbital is antisymmetric with respect to the plane bisecting the two hydrogen atoms and hence has p_y character. Consequently, the correlation of these orbitals to form the N–N bond of N_2H_4 is sometimes referred to as π-like (e.g., Ref. 21). We prefer to call it a σ bond in order to avoid confusion with the p_z–p_z correlation which forms an unambiguous π bond for planar N_2H_4.
[67] R. S. Mulliken, J. Chem. Phys. **66**, 2448 (1977); **71**, 556 (1979); A. J. Merer and R. S. Mulliken, Chem. Rev. **69**, 639 (1969).
[68] L. E. McMurchie and E. R. Davidson, J. Chem. Phys. **67**, 5613 (1978); R. J. Buenker, S. D. Peyerimhoff, and W. E. Kammer, *ibid.* **55**, 814 (1971).
[69] M. B. Robin, *Higher Excited States of Polyatomic Molecules*, Vol. II (Academic, New York, 1975), pp. 1 ff.
[70] M. B. Robin, *Higher Excited States of Polyatomic Molecules*, Vol. III (Academic, New York, 1985), pp. 213 ff.
[71] J. W. Rabalais, *Principles of Ultraviolet Photoelectron Spectroscopy* (Wiley, New York, 1977), p. 99 ff.
[72] The assignments by Robin (Ref. 69, pp. 314–5) and Staemmler (Ref. 24) were made without knowledge of the 178 and 218 nm band which were first revealed in Ref. 14 and in this work.